Exciton Characteristics in Graphene Epoxide

Xi Zhu[†] and Haibin Su[†,‡,*]

[†]Division of Materials Science, Nanyang Technological University, 50 Nanyang Avenue, 639798 Singapore, and [‡]Institute of Advanced Studies, Nanyang Technological University, 60 Nanyang View, 639673 Singapore

ABSTRACT Exciton characteristics in graphene epoxide (GE) are investigated by density functional theory with quasi-particle corrections and many-body interactions. The nature of the exciton is influenced by epoxide content and detailed geometric configurations. Two kinds of excitons are identified in GE: Frenkel-like exciton originated from the sp^2 carbon cluster and charge-transfer exciton formed by localized states involving both oxygen and carbon atoms. The unusual blue shift associated with the Frenkel-like exciton leaking is highlighted. One scaling relationship is proposed to address the power-law dependence of Frenkel-like exciton binding strength on its size. The charge-transfer exciton appears in GE samples with the high oxygen coverage. Particularly, the exciton in GE structures exhibits long lifetime by analyzing both radiative and nonradiative decay processes. This study sheds light on the potential applications of GE-based structures with attractive high quantum yield in light emission and optoelectronic technology.

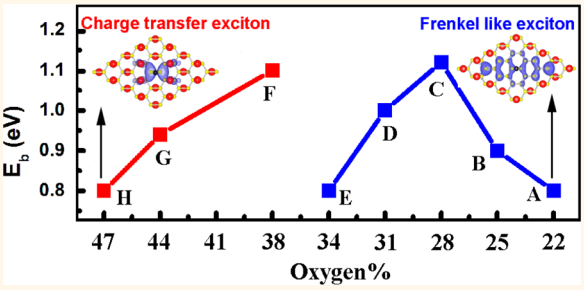

KEYWORDS: graphene epoxide · charge-transfer exciton · Frenkel-like exciton

Originally discovered by Benjamin Brodie in 1859,[1] graphene oxide (GO) is a chemically derived graphene structure with sheet thickness around 0.6 nm as measured by the neutron scattering method on dehydrated samples[2] that together with its reduced form (rGO) has recently attracted great attention due to its potential versatile applications particularly in the optical and optoelectronic technology, as discussed in recent reviews.[3,4] Extensive experimental characterizations including solid-state nuclear magnetic resonance have shown that hydroxyl and epoxide groups spread across the basal planes, while carboxyl and carbonyl groups exist at edge sites.[5−7] However, the nonstoichiometric chemical composition and structural inhomogeneity of GO impose the formidable challenge of determining the precise atomic structure of GO samples.[8−10] Interestingly, recent studies of the photoluminescence (PL) in GO have revealed the versatile characteristics in near-infrared, visible, and ultraviolet fluorescence.[11−15] The tunable PL together with biocompatibility makes GO highly attractive for biological applications.[16] Despite the enormous efforts on the origin of PL in GO, the desirable understanding is still lacking. For instance, the broad luminescence from 400 to 800 nm in the oxygen plasma-treated, mechanically exfoliated monolayer graphene sheet exhibits homogeneous characteristics that result from broadening of emission species containing both carbon and oxygen atoms.[12] However, the subpicosecond time-resolved PL measurements show that the ultrafast spectral migration occurs among the emitting states to broaden the PL spectrum inhomogeneously in GO within a few picoseconds.[17] Moreover, the blue luminescence with a narrow bandwidth from the chemically reduced GO (rGO) by hydrazine is attributed to the graphitic domains of sp^2 clusters because the observed enhancement of blue luminescence with reduction suggests that oxygen functional groups can be excluded as the origin.[13,14] One new twist has just been added from the remarkable observation by Matsuda and co-workers of the coexistence of emission species in GO with both blue and UV PL.[15] Clearly, the versatile yet strongly heterogeneous atomic structure of GO limits the comprehensive analysis of the origin of its PL.

* Address correspondence to hbsu@ntu.edu.sg.

Received for review August 31, 2013 and accepted January 24, 2014.

Published online January 24, 2014
10.1021/nn404563k

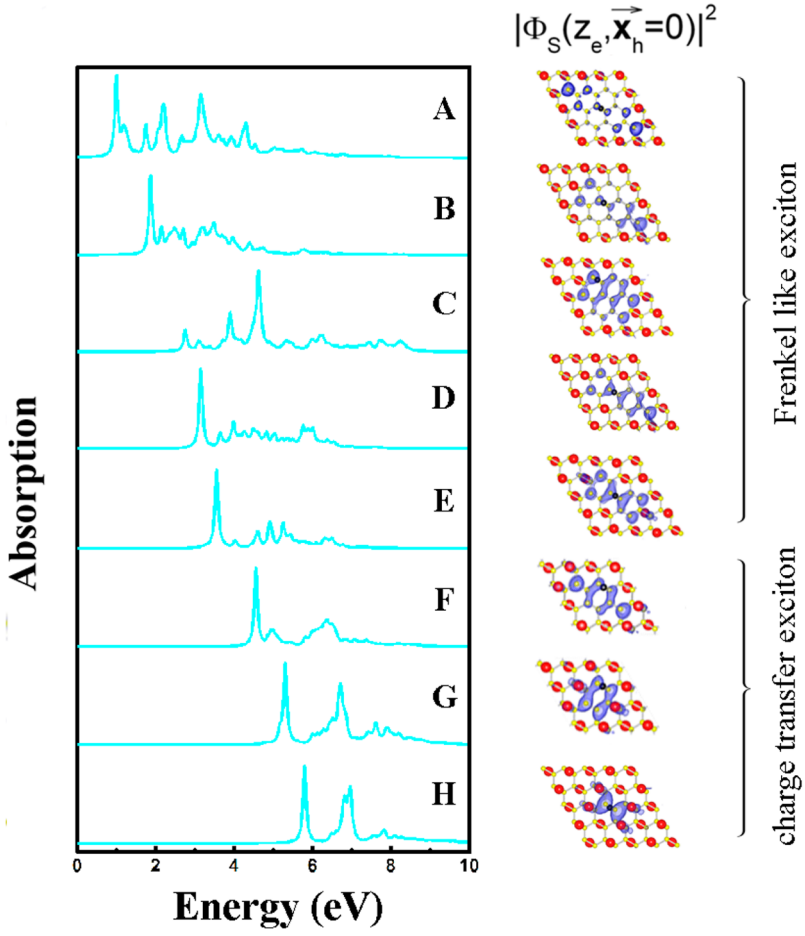

Figure 1. Computed absorption spectra and the square of exciton wave functions (blue) of eight GE structures. The gray and red balls represent carbon and oxygen atoms, respectively. The excitons in GE structures A−E are Frenkel-like, while charge-transfer excitons exist in GE structures F−H.

One remarkable method to fabricate graphene epoxide (GE) has been developed by Hersam and coworkers.[18] The atomic oxygen produced by thermal cracking of O_2 molecules chemisorbs to the basal plane of graphene to form GE in ultrahigh vacuum conditions. The chemisorbed oxygen can be laterally translocated by the STM tip, which paves the way to generate well-defined GE composition and structure. This type of GE material with atomic precision is ideal for the study of the optical properties. The understanding of the microscopic origin of exciton in GE can also be applicable to GO. In this work, we investigate the origin and characteristics of exciton in GE using density functional theory with quasi-particle correction and explicit electron−hole interaction which is included by solving the Bethe−Salpeter equation in the basis set of quasi-electron and quasi-hole states within the random-phase approximation.[19−21] There are two kinds of excitons in GE: Frenkel-like exciton (FE) originated from the sp^2 carbon cluster and charge-transfer exciton (CTE) formed by localized electronic states involving both oxygen and carbon atoms. The scaling relation between the FE exciton binding energy and its size is proposed, which presents a different exponent as compared with carbon nanotubes and graphene nanoribbons. Both radiative and phonon-assisted nonradiative dynamic processes are addressed to unravel the promising potential of GE as strategically important materials in optical and optoelectronics technology.

RESULTS AND DISCUSSION

Eight oxygen content dependent GE structures are constructed by forming expoxy groups in the 4 × 4 graphene unit cells, as shown in the Figure 1, together with wave functions (see Supporting Information Figure S2 for enlarged structural details). The size of the confined sp^2 carbon area in GE structures has been characterized *via* STM from less than 1 nm to 5 nm.[18] The oxygen concentration, represented by O/C ratio, ranges from 22% (structure A) to 47% (structure H). The distribution of epoxide in the structures studied in this work is in good agreement with that reported by Yan *et al.*[22] The epoxide groups energetically prefer to aggregate and form stripes on opposite sides of the graphene basal plane to compensate the buckling (as demonstrated in Supporting Information Figure S1). When these structures are synthesized, the solid-state

NMR can be very helpful to characterize the structural details as demonstrated in the studies of GO structure.[5,7] The simulated absorption spectra of all GE structures studied in this work are plotted in Figure 1. For the structures from A to E with oxygen coverage below 35%, all epoxide groups confine the sp^2 carbon to form localized carbon domains. The number of sp^2 carbon atoms can be used to represent the size of confined carbon domain. For these structures (A−E), the square of Frenkel-like exciton wave functions as presented in Figure 1, together with the square of wave functions of valence band maximum (VBM) and conduction band minimum (CBM) as shown in Supporting Information Figure S7, clearly presents the predominant π and π^* character. The quantum confinement results in the increase of optical absorption energy (E_a) as listed in Table 1. For the structures from F to H with high O/C ratio above 35%, the VBM wave functions have more oxygen 2p orbital character, while the carbon p_z orbital contributes largely to CBM wave functions. Consequently, the energy levels of VBM reduce by 0.3 eV, as compared with more than double increase (0.8 eV) of CBM energies (see Supporting Information Figure S6). Thus, the further blue shift in E_a as the O/C ratio increases, as shown in Table 1, results from the synergized effects with relatively more confinement of the CBM in gap opening as presented in Figure 1. The square of exciton wave functions of structures F−H, as presented in Figure 1, together with the corresponding analysis in Supporting Information Figure S7, exhibits the appreciable charge transfer upon the excitation.

We now address two kinds of excitons in GE structures as revealed in the present study: Frenkel-like exciton originating from the sp^2 carbon cluster and charge-transfer exciton formed by localized electronic states involving both oxygen and carbon atoms. The formation of the exciton state leads to significant spectral transfer from interband transition to the sharp exciton one. The exciton binding energy, E_b, is defined as the difference between the GW band gap and the optical absorption energy (*i.e.*, $E_b = E_g^{GW} - E_a$). The exciton binding energy (E_b) dependence on the oxygen coverage in GE is presented in Figure 2. The analysis of exciton wave function of FE shows the clear origin of the sp^2 carbon atoms. Take structure A, for example; the confined carbon domain has 18 sp^2 carbon atoms, and the exciton wave functions have remarkable p_z character (see the inset at the top right corner of Figure 2). From structure A to C, E_b increases with decreasing number of sp^2 carbon atoms. The excitation is from π to π^* in the sp^2 carbon cluster, which has the same orbital feature as single-walled carbon nanotubes (SWCNTs),[23,24] graphene nanoribbons with armchair edges (AGNR),[25,26] and graphene quantum dots.[27] The spatial localization of FE is largely contributed from VBM and CBM. Intriguingly, the exciton binding strength is reduced from structure C to E.

TABLE 1. Computed Band Gap, E_g^{GW} (with GW Method), Optical Absorption Energy, E_a (with Bethe−Salpeter Method), and Exciton Binding Energy, E_b, of GE Structures (A−H) in Electronvolts

	A	B	C	D	E	F	G	H
E_g^{GW}	1.89	2.83	3.90	4.20	4.41	5.60	6.14	6.7
E_a	1.09	1.93	2.78	3.2	3.61	4.50	5.20	5.90
E_b	0.80	0.90	1.12	1.00	0.80	1.10	0.94	0.80

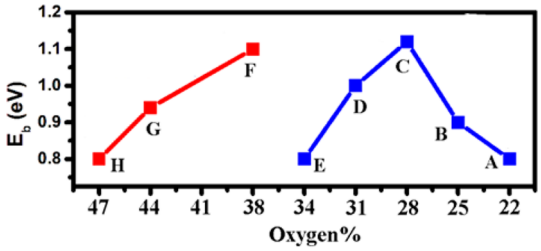

Figure 2. Exciton binding strength (E_b) as a function of oxygen coverage in GE. The blue (red) points refer to data of Frenkel-like (charge-transfer) exciton. Data points of the same type of exciton are connected by line segments to present the general trend.

This phenomenon is attributed to the leakage of exciton wave function outside of the boundary made of epoxide groups, as shown in Figure 1. Remarkably, the leakage leads to the blue shift in the absorption spectra changes from structure C to E, in contrast to the usual observation of leakage-induced red shift in the absorption spectra.[28] To unravel the microscopic origin of the confinement and leakage phenomena, we chose a series of polycyclic aromatic hydrocarbons (PAHs) to model the sp^2 carbon cluster region in the GE structures embedded inside the epoxide-rich region. As shown in Supporting Information Figure S6, oxygen coverage has a strong influence on the work function of GE. Thus, we chose the structure H to model the expoxide-rich boundary for capturing the heterogeneous character of structures A−E. To align the energy levels, we compute work function/VBM/CBM of GE structure H and ionization potential and electron affinity of PAH molecules, as shown in Supporting Information Table S1.

Subsequently, the aligned energy levels of the epoxide-rich region of GE together with PAHs are presented in Figure 3. The HOMO energy level decreases from −6.06 eV in $C_{42}H_{16}$ to −7.12 eV in $C_{16}H_6$, while the LUMO level increases from −1.22 to −0.45 eV accordingly, which shows a nice correlation with the size of PAHs. Similar relation has been proposed for the linear polyacenes by both half-wave reduction potential measurement[29] and AM1 semiempirical computations.[30] The LUMO positions of PAHs are above the CBM of the epoxide-rich region. However, HOMO levels of both coronene ($C_{24}H_{12}$) and pyrene ($C_{16}H_{10}$) are below the VBM level of the epoxide-rich region. Thus, the leakage of

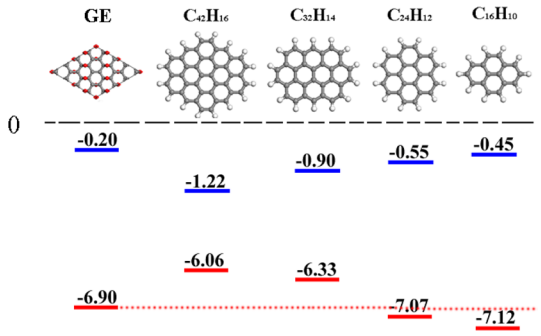

Figure 3. Alignment of energy levels of GE and PAH molecules in units of electronvolt. The vacuum level is set to be zero. The red (blue) levels represent VBM/HOMO (CBM/LUMO) energy levels of these structures.

FE is featured with the prevailing hole component. This leakage leads to the reduction of exciton binding energy in structures D and E. To quantify the confinement effect on exciton, we plot the exciton binding strength (E_b) as a function of the size of exciton (L) for structures A−E in Figure 4. For structures A−C, L is very close to the size of sp^2 carbon region, while for structures D and E, due to the leakage of the exciton wave function, the value of L goes beyond the spatial length of the confined sp^2 carbon region. By analyzing the power-law dependence of E_b and L in structures A−E (*i.e.*, $E_b \sim L^{\delta}$), an exponent value of −0.83 is obtained, with reference to the exponent of −1 for SWCNTs,[23,24] and three distinct exponents of −1.0, −0.91, and −1.80 for AGNRs with 3p, 3p+1, and 3p+2 families, respectively.[25] Compared with the quasi-1D SWCNTs and AGNRs, the sp^2 carbon region of GE structures has more localized electronic structure and very weak screening strength, which leads to the lower exponent value. The poor screening characteristics of the sp^2 carbon region of GE is very different from the strong shielding of quantum dots, due to the fact that the former is the zero dimension limit of the quasi-1D while the latter is with respect to 3D.[31] The wavelength of PL from FE is tunable in the IR and visible regions by manipulating the size of the sp^2 carbon cluster. For structures F−H, the VBM and CBM are distributed on epoxide and sp^2 carbon region, respectively. A charge-transfer character is thus expected for this excitation, similar to CTE in graphene nanojunctions[32] and donor−acceptor interfaces of organic materials.[33] The first absorption peak with prominent charge-transfer character is contributed by the combination of VBM/CBM and orbitals of higher energy with appreciable amount of oscillator strength. The larger GW gap of structure F leads to the heavier reduced mass and weaker screening, which accounts for the stronger binding strength than that of structure E, as shown in Figure 2. As discussed previously, the GW gap increases from structure F to H. However, the polarization strength associated with the charge transfer from carbon to oxygen gets enhanced with the increase of the oxygen coverage. Therefore, the strong coupling between CTE and the polar groups

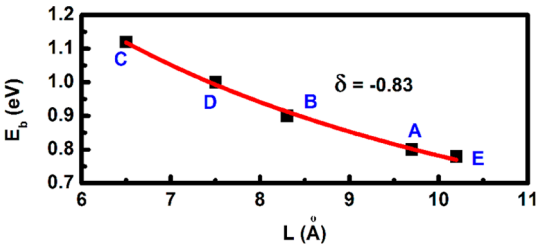

Figure 4. Scaling relationship between the binding energy (E_b) of Frenkel-like exciton and its size (L) in GE structures A−E (*i.e.*, $E_b \sim L^{\delta}$).

reduces the CTE binding strength as increasing oxygen coverage.

The potential of GE as optical materials depends on the luminescence efficiency, which is determined by both radiative and nonradiative lifetimes. The radiative decay rate (inverse of radiative lifetime, τ_r) for each excitonic state is[34]

$$\frac{1}{\tau_r} = \frac{ne^2E_a^2f}{2\pi\varepsilon m_e\hbar^2c^3} \quad (1)$$

where e, m_e, $\hbar$, c, and n are charge and rest mass of electron, Plank's constant divided by 2π, speed of light, and the refractive index (hereafter n = 1.8[35]), respectively. Taking the surrounding medium's dielectric constant ε to be 3.2, and using the calculated optical absorption energy (E_a) and the corresponding oscillator strengths (f), we estimate that the radiative lifetime is longer than 3 ns. To address the remarkable high-energy optical phonon mode assisted energy relaxation process, we compute the nonradiative decay rate (inverse of nonradiative lifetime, τ_n) with the following formula[36]

$$\frac{1}{\tau_n} = \frac{2\pi}{\hbar}\frac{S^{N-1}}{\pi(N-1)!}e^{-S}\frac{N^2\gamma S_l(\hbar w)^2}{(E_a - N\hbar w)^2 + (N\gamma)^2} \quad (2)$$

where N is the number of phonons, $\hbar w$ is the optical phonon, γ is the broadening, and S and S_l are interband and intraband Huang−Rhys factor. Multiphonon decay of an exciton is a possible mechanism in GE when considering that the optical phonon energy could be comparable to the optical band gaps. As the nonradiative lifetime is closely dependent on Huang−Rhys factors, the detail analysis of electron−phonon coupling should be addressed to gain better understanding of the effects of GE structures on charge dynamics. The interaction between electron and phonon, λ, is computed by density functional perturbation theory.[37] The electron−phonon coupling strength gradually increases due to the confinement effect for the sp^2 carbon cluster (see Supporting Information Figure S8). Besides, the phonon modes involving oxygen atoms especially in the structures with high oxygen content result in the further enhancement of electron−phonon coupling. Thus, as compared with the weak electron−phonon coupling of 0.14 in the sp^2 carbon cluster

region of GE, the electron−phonon coupling strength is as high as 0.65 in the epoxide-rich GE structures (see Supporting Information Figure S9). The strong electron−phonon coupling plays an important role in promoting dynamic processes to facilitate the delicate energy-transfer process. Choosing 200 meV as the optical phonon energy, 20 meV as the broadening parameter, and 1.0 for both interband and intraband Huang−Rhys factors, we estimate that the exciton lifetime due to the multiphonon decay mechanism is longer than 100 ps. Thus, GE-based light-emitting devices can be expected to have high quantum yield owing to the long lifetime of excitons. In addition to electron−phonon effect, there is another important factor, that is, the impurity level induced by the disorder states, which affects the optical properties of GE structures. The likely coexistence of an ensemble of configurations with similar energy in GE samples especially with high oxygen coverage generates an assortment of impurity levels. The disorder-induced states likely act as the impurity levels inside band gaps. These localized impurity states participate in the light absorption, energy relaxation dynamics, and light emission leading to the PL spectrum. As shown in recent studies on GO,[3,11] the pump−probe experiments are anticipated to play a key role in investigating the exciton dynamics of GE structures. Therefore, the interplay between electron−phonon and disorder will have profound influence on the characteristics of PL in GE structures.

CONCLUSIONS

In summary, inspired by the remarkable synthesis method of high-quality GE samples, the exciton characteristics of GE are scrutinized to uncover its application potential in optical and optoelectronics technology. For the epoxide content below 35%, FE is dominated as featured in the sp^2 carbon cluster region. The leaking of FE is observed for the epoxide content between 30 and 35% O/C ratio. The unusual blue shift associated with the FE leaking is highlighted. The power law is proposed to address the dependence of FE binding strength on its size, which unravels much weaker shielding strength of the π electron in the sp^2 carbon cluster of GE samples than that in SWCNTs and AGNRs. The CTE, formed by localized states involving both oxygen and carbon atoms, appears in GE samples with the high epoxide content. The long lifetime of exciton in GE structures is highly desirable, which makes the development of GE-based light emission and optoelectronic technology very appealing.

METHODS

We employ the density functional theory with quasi-particle correction and explicit electron−hole interaction, which is included by solving the Bethe−Salpeter equation in the basis set of quasi-electron and quasi-hole states within the random-phase approximation[18−21]

$$(E_{ck} - E_{vk})A^S_{vck} + \sum_{k'v'c'} \langle vck|K^{eh}|v'c'k'\rangle A^S_{v'c'k'} = \Omega^S A^S_{vck} \quad (3)$$

where A^S_{vck} is the exciton wave function, K^{eh} is the electron−hole coupling kernel, Ω^S is the excitation energy, and E_{ck} and E_{vk} are the quasi-particle energy of the electron and hole states, respectively. Since the supercell method is used for the nonbulk structures, a box-shape truncated Coulomb interaction on the z axis is applied to eliminate the image effect between adjacent supercells to mimic isolated low-dimensional structures.[38,39] A total of 10 bands with the Fermi level lying between are chosen in our calculations. The interaction between electron and phonon, λ, is computed as[37,40]

$$\lambda = 2\int_0^\infty d\omega \sum_{k,q,v,n,m} \frac{\delta(\varepsilon^n_k)\delta(\varepsilon^m_{k+q})}{N(E_F)} |g^{v,n,m}_{k,k+q}|^2 \delta(\omega - \omega_{vq})/\omega \quad (4)$$

where $g^{v,n,m}_{k,k+q}$ are the electron−phonon matrix elements that are averaged along the Fermi surface $\delta(\varepsilon^n_k)$. $N(E_F)$ is the density of states on the Fermi surface.

Conflict of Interest: The authors declare no competing financial interest.

Acknowledgment. We are grateful for the fruitful discussions with Manish Chhowalla at Rutgers University; Kazunari Matsuda at Kyoto University; Jay Kikkawa at UPenn; Mark Hersam at Northwestern University; and Zhengyu Li, Qunxiang Li, and Jinglong Yang at USTC. H.B.S. thanks the Institute of Natural Sciences in Shanghai for the kind hospitality where part of this manuscript was prepared. Work at NTU was supported in part by National Research Foundation (Grant No. NRF-CRP9-2011-04) and A*STAR SERC (Grant No. 1121202012).

Supporting Information Available: Details of the computation methods, structures of GE, energy levels/square of wave functions of CBM and VBM, oxygen coverage dependent work function of GE, IP/EA of PAH molecules, and the electron−phonon coupling. This material is available free of charge *via* the Internet at http://pubs.acs.org.

REFERENCES AND NOTES

1. Brodie, B. C. On the Atomic Weight of Graphite. *Philos. Trans. R. Soc. London* **1859**, *149*, 249–259.
2. Buchsteiner, A.; Lerf, A.; Pieper, J. Water Dynamics in Graphite Oxide Investigated with Neutron Scattering. *J. Phys. Chem. B* **2006**, *110*, 22328–22338.
3. Eda, G.; Chhowalla, M. Chemically Derived Graphene Oxide: Towards Large-Area Thin-Film Electronics and Optoelectronics. *Adv. Mater.* **2010**, *22*, 2392–2415.
4. Loh, K. P.; Bao, Q. L.; Eda, G.; Chhowalla, M. Graphene Oxide as a Chemically Tunable Platform for Optical Applications. *Nat. Chem.* **2010**, *2*, 1015–1024.
5. Lerf, A.; He, H. Y.; Forster, M.; Klinowski, J. Structure of Graphite Oxide Revisited. *J. Phys. Chem. B* **1998**, *102*, 4477–4482.
6. Szabo, T.; Berkesi, O.; Forgo, P.; Josepovits, K.; Sanakis, Y.; Petridis, D.; Dekany, I. Evolution of Surface Functional Groups in a Series of Progressively Oxidized Graphite Oxides. *Chem. Mater.* **2006**, *18*, 2740–2749.
7. Cai, W. W.; Piner, R. D.; Stadermann, F. J.; Park, S.; Shaibat, M. A.; Ishii, Y.; Yang, D. X.; Velamakanni, A.; An, S. J.; Stoller, M.; *et al.* Synthesis and Solid-State NMR Structural Characterization of ^{13}C-Labeled Graphite Oxide. *Science* **2008**, *321*, 1815–1817.
8. Dreyer, D. R.; Park, S.; Bielawski, C. W.; Ruoff, R. S. The Chemistry of Graphene Oxide. *Chem. Soc. Rev.* **2010**, *39*, 228–240.

9. Bagri, A.; Mattevi, C.; Acik, M.; Chabal, Y. J.; Chhowalla, M.; Shenoy, V. B. Structural Evolution during the Reduction of Chemically Derived Graphene Oxide. *Nat. Chem.* **2010**, *2*, 581–587.
10. Lu, N.; Huang, Y.; Li, H. B.; Li, Z. Y.; Yang, J. L. First Principles Nuclear Magnetic Resonance Signatures of Graphene Oxide. *J. Chem. Phys.* **2010**, *133*, 034502.
11. Luo, Z. T.; Vora, P. M.; Mele, E. J.; Johnson, A. T. C.; Kikkawa, J. M. Photoluminescence and Band Gap Modulation in Graphene Oxide. *Appl. Phys. Lett.* **2009**, *94*, 111909.
12. Gokus, T.; Nair, R. R.; Bonetti, A.; Bohmler, M.; Lombardo, A.; Novoselov, K. S.; Geim, A. K.; Ferrari, A. C.; Hartschuh, A. Making Graphene Luminescent by Oxygen Plasma Treatment. *ACS Nano* **2009**, *3*, 3963–3968.
13. Eda, G.; Lin, Y. Y.; Mattevi, C.; Yamaguchi, H.; Chen, H. A.; Chen, I. S.; Chen, C. W.; Chhowalla, M. Blue Photoluminescence from Chemically Derived Graphene Oxide. *Adv. Mater.* **2010**, *22*, 505.
14. Chien, C. T.; Li, S. S.; Lai, W. J.; Yeh, Y. C.; Chen, H. A.; Chen, I. S.; Chen, L. C.; Chen, K. H.; Nemoto, T.; Isoda, S.; *et al.* Tunable Photoluminescence from Graphene Oxide. *Angew. Chem., Int. Ed.* **2012**, *51*, 6662–6666.
15. Kozawa, D.; Miyauchi, Y.; Mouri, S.; Matsuda, K. Exploring the Origin of Blue and Ultraviolet Fluorescence in Graphene Oxide. *J. Phys. Chem. Lett.* **2013**, *4*, 2035–2040.
16. Liu, Z.; Robinson, J. T.; Sun, X. M.; Dai, H. J. PEGylated Nanographene Oxide for Delivery of Water-Insoluble Cancer Drugs. *J. Am. Chem. Soc.* **2008**, *130*, 10876.
17. Exarhos, A. L.; Turk, M. E.; Kikkawa, J. M. Ultrafast Spectral Migration of Photoluminescence in Graphene Oxide. *Nano Lett.* **2013**, *13*, 344–349.
18. Hossain, M. Z.; Johns, J. E.; Bevan, K. H.; Karmel, H. J.; Liang, Y. T.; Yoshimoto, S.; Mukai, K.; Koitaya, T.; Yoshinobu, J.; Kawai, M.; *et al.* Chemically Homogeneous and Thermally Reversible Oxidation of Epitaxial Graphene. *Nat. Chem.* **2012**, *4*, 305–309.
19. Godby, R. W.; Needs, R. J. Metal-Insulator-Transition in Kohn-Sham Theory and Quasiparticle Theory. *Phys. Rev. Lett.* **1989**, *62*, 1169–1172.
20. Rohlfing, M.; Louie, S. G. Electron−Hole Excitations and Optical Spectra from First Principles. *Phys. Rev. B* **2000**, *62*, 4927–4944.
21. Marini, A.; Hogan, C.; Gruning, M.; Varsano, D. YAMBO: An *Ab Initio* Tool for Excited State Calculations. *Comput. Phys. Commun.* **2009**, *180*, 1392–1403.
22. Yan, J. A.; Xian, L. D.; Chou, M. Y. Structural and Electronic Properties of Oxidized Graphene. *Phys. Rev. Lett.* **2009**, *103*, 086802.
23. Perebeinos, V.; Tersoff, J.; Avouris, P. Scaling of Excitons in Carbon Nanotubes. *Phys. Rev. Lett.* **2004**, *92*, 257402.
24. Dukovic, G.; Wang, F.; Song, D. H.; Sfeir, M. Y.; Heinz, T. F.; Brus, L. E. Structural Dependence of Excitonic Optical Transitions and Band-Gap Energies in Carbon Nanotubes. *Nano Lett.* **2005**, *5*, 2314–2318.
25. Zhu, X.; Su, H. B. Scaling of Excitons in Graphene Nanoribbons with Armchair Shaped Edges. *J. Phys. Chem. A* **2011**, *115*, 11998–12003.
26. Zhu, X.; Su, H. B. Excitons of Edge and Surface Functionalized Graphene Nanoribbons. *J. Phys. Chem. C* **2010**, *114*, 17257–17262.
27. Peng, J.; Gao, W.; Gupta, B. K.; Liu, Z.; Romero-Aburto, R.; Ge, L. H.; Song, L.; Alemany, L. B.; Zhan, X. B.; Gao, G. H.; *et al.* Graphene Quantum Dots Derived from Carbon Fibers. *Nano Lett.* **2012**, *12*, 844–849.
28. Dabbousi, B. O.; RodriguezViejo, J.; Mikulec, F. V.; Heine, J. R.; Mattoussi, H.; Ober, R.; Jensen, K. F.; Bawendi, M. G. (CdSe)ZnS Core−Shell Quantum Dots: Synthesis and Characterization of a Size Series of Highly Luminescent Nanocrystallites. *J. Phys. Chem. B* **1997**, *101*, 9463–9475.
29. Streitwieser, A. *Molecular Orbital Theory for Organic Chemists*; John Wiley and Sons Inc.: New York, 1961.
30. Notario, R.; Abboud, J. L. M. Probing the Limits of Resonance Stabilization. The Case of Linear Polyacenes. *J. Phys. Chem. A* **1998**, *102*, 5290–5297.
31. Bawendi, M. G.; Steigerwald, M. L.; Brus, L. E. The Quantum-Mechanics of Larger Semiconductor Clusters (Quantum Dots). *Annu. Rev. Phys. Chem.* **1990**, *41*, 477–496.
32. Cocchi, C.; Prezzi, D.; Ruini, A.; Caldas, M. J.; Molinari, E. Optical Properties and Charge-Transfer Excitations in Edge-Functionalized All-Graphene Nanojunctions. *J. Phys. Chem. Lett.* **2011**, *2*, 1315–1319.
33. Jailaubekov, A. E.; Willard, A. P.; Tritsch, J. R.; Chan, W. L.; Sai, N.; Gearba, R.; Kaake, L. G.; Williams, K. J.; Leung, K.; Rossky, P. J.; *et al.* Hot Charge-Transfer Excitons Set the Time Limit for Charge Separation at Donor/Acceptor Interfaces in Organic Photovoltaics. *Nat. Mater.* **2013**, *12*, 66–73.
34. Feldmann, J.; Peter, G.; Göbel, E. O.; Dawson, P.; Moore, K.; Foxon, C.; Elliott, R. J. Linewidth Dependence of Radiative Exciton Lifetimes in Quantum Wells. *Phys. Rev. Lett.* **1987**, *59*, 2337–2340.
35. Jung, I.; Vaupel, M.; Pelton, M.; Piner, R.; Dikin, D. A.; Stankovich, S.; An, J.; Ruoff, R. S. Characterization of Thermally Reduced Graphene Oxide by Imaging Ellipsometry. *J. Phys. Chem. C* **2008**, *112*, 8499–8506.
36. Perebeinos, V.; Avouris, P. Phonon and Electronic Nonradiative Decay Mechanisms of Excitons in Carbon Nanotubes. *Phys. Rev. Lett.* **2008**, *101*, 057401.
37. Giannozzi, P.; Baroni, S.; Bonini, N.; Calandra, M.; Car, R.; Cavazzoni, C.; Ceresoli, D.; Chiarotti, G. L.; Cococcioni, M.; Dabo, I.; *et al.* QUANTUM ESPRESSO: A Modular and Open-Source Software Project for Quantum Simulations of Materials. *J. Phys.: Condens. Matter* **2009**, *21*, 395502.
38. Ismail-Beigi, S. Truncation of Periodic Image Interactions for Confined Systems. *Phys. Rev. B* **2006**, *73*, 233103.
39. Rozzi, C. A.; Varsano, D.; Marini, A.; Gross, E. K. U.; Rubio, A. Exact Coulomb Cutoff Technique for Supercell Calculations. *Phys. Rev. B* **2006**, *73*, 205119.
40. Allen, P. B.; Dynes, R. C. Transition-Temperature of Strong-Coupled Superconductors Reanalyzed. *Phys. Rev. B* **1975**, *12*, 905–922.